Bull. Fac. Bioresources, Mie Univ.
No.31 : 1－23
March 15, 2004

A Numerical Experiment on a New Current, the Ryukyu Current Extension, in the Shikoku Basin Part I Linear and Weak Nonlinear Model

Yoshihiko SEKINE*

Faculty of Bioresources, Mie University, 1515 Kamihamachou, Tsu, Mie 514-8507 Japan

Abstract

The existence of two western boundary currents along the eastern continental slopes off the Nansei Islands (Ryukyu Current) and the Izu Ridge in the subtropical circulation in the North Pacific has been pointed out to occur from late winter to spring due to the barotropic ocean response being dominant for seasonal variations in wind stress. As a results, a new connecting new current from the Ryukyu Current to the western boundary current east of the Izu Ridge is predicted, which is referred to as the Ryukyu Current Extension. In order to see the flow characteristics of the Ryukyu Current Extension, some numerical experiments are carried out with a barotropic flat bottom model driven by Sverdrup in-and outflow in winter and in spring. The results of the numerical experiment with a linear and weak nonlinear parameters are presented in the present paper. It is shown that there exist four types of the current patterns in the Shikoku Basin: the Munk Pattern, the Moore Pattern, the Nonlinear Pattern and the Super Nonlinear Pattern. In case with the larger eddy viscosity, only the Munk Pattern is formed. If the eddy viscosity is decreased, the Moore Pattern is formed in the small in- and outflow models (deep models), while the Nonlinear Pattern appears in large in- and outflow models (shallow models) and the Super Nonliar Pattern in the largest in- and outflow model (shallowest model). It is also shown that the formation of the Ryukyu Current Extension is clear in cases of the Moore and Munk Patterns, but unclear in cases of the Nonlinear and Super Nonlinear Patterns.

Key Words: Ryukyu Current, western boundary current, numerical ocean modeling

1. Introduction

So far, some numerical studies (e. g., Sekine and Kutsuwada[1]; Kagimoto and Yamagata[2]) examined seasonal variations in volume transport of the Kuroshio and it is commonly pointed out that the Kuroshio has a maximum transport in late winter and a minimum transport from summer to early autumn. The time lag between the calculated transport and the Sverdrup transport is about one month, which shows that the barotropic response is dominant for the seasonal change in the wind stress over the North Pacific. Because the barotropic flow has a tendency to flow along the contour of f/h[3),4)], where f is a Coriolis parameter and h is a depth of ocean, a western boundary current is formed along the eastern continental

Accepted: October 30, 2003

* For correspondence (e-mail: sekine@bio.mie-u.ac.jp)

slope off Nansei Islands south of Kyushu, which has been referred to the Ryukyu Current.

Recent detailed observations of the volume transport of the Kuroshio off Shikoku (e. g., Imawaki et al.[5]) show that the Kuroshio has a small seasonal variation in the volume transport with a weak peak in summer. Therefore, the observed seasonal variation in the volume transport of the Kuroshio is significantly different from that of the Sverdrup transport and the calculated transport with a maximum in winter and a minimum in summer. As for the different seasonal variation between the two transport, Isobe and Imawaki[6] numerically showed that the different seasonal variation is due to the topographic effect of the Izu Ridge that blocks the westward propagation of the barotropic Rossby wave.

As for the actual ocean response in the North Pacific, Kawabe[7] examined the westward propagation of the Rossby wave formed by the observed wind stress and showed the volume transport of the western boundary currents (Fig. 1). He pointed out that the volume transport of the Ryukyu Current (31 Sv: 1 Sv$=10^6$ m^{3}sec^{-1}) is larger than that of the ordinary Kuroshio flow (26 Sv) in the East China Sea. Here, as he considered topographic effects of the Izu-Ogasawara Trench, a southward western boundary current with a transport of 7 Sv is shown in. Since the eastward current from Ryukyu Current to the western boundary current along the eastern side of the Izu-Ogasawara Trench is suggested by the mass conservation, Kawabe[7] implies the existence of the subtropical counter current pointed out by Hasunuma and Yoshida[8], which is also shown in.

It is inferred from the zonal movement of mesoscale eddies[9, 10] and the distribution of the North Pacific Intermediate water south of Japan[11, 12] that the topographic effect of the Izu-Ogasawara Trench is rather small, while the topographic effect of the Izu Ridge is important and the barotropic western boundary

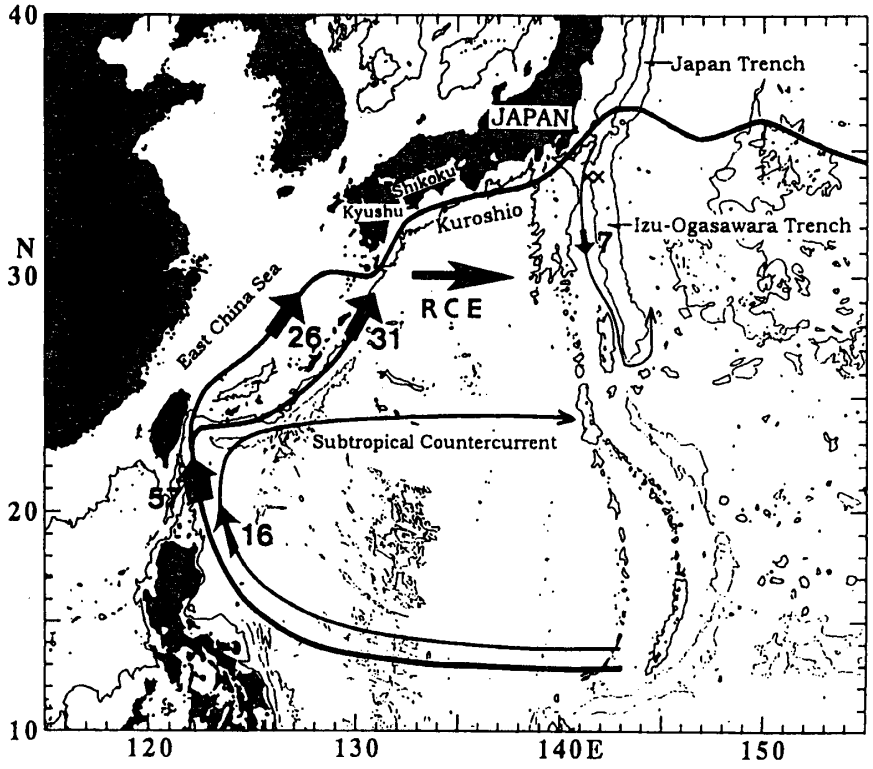

Fig. 1 Volume transport of the wind driven western boundary current estimated by Kawave (2001)[7]. A predicted new current, the Ryukyu Current Extension, is also shown by the large arrow marked by RCE.

current is formed in the eastern side of the Izu Ridge in north to 30° N. It is expected that there exists a connecting current between the Ryukyu Current and the western boundary current along the eastern side of the Izu Ridge in the Shikoku Basin. As this current is an extension of the Ryukyu Current, it is hereafter referred to as the Ryukyu Current Extension, which is schematically shown by the large arrow in.

Since the Indian Ocean and the Atlantic Ocean are connected at the southern tip of Africa, the subtropical circulation spreads to both oceans. Therefore, there exsists a western boundary current followed by a separating current around Africa and a western boundary current along the eastern continental slope of South America. They corresponds to the Benguela Current and the Agulhas Current in the former case and the Brazil Current in the latter case.

Dynamics of the subtropical circulation in the Indian Ocean and the Atlantic Ocean and the associated western boundary currents was numerically examined by DeRuijter[13] and DeRuijter and Boudra[14]. They showed the various flow pattern of these currents depending on the intensity of the advection (nonlinearity) and eddy viscosity. However, since the horizontal scale of the Shikoku Basin is significantly small compared with that of the subtropical circulation in the Indian Ocean and the Atlantic Ocean, detailed discussion on the dynamics of the Ryukyu Current Extension should be made independently.

In the present study, some numerical experiments on the Ryukyu Current Extension are carried out and the results of the numerical experiments with the linear and weak nonlinear parameter range are presented, as the first step of the numerical experiment on the Ryukyu Current Extension. In the following, description of the numerical model will be made in the next section. Results of the numerical experiments will be mentioned in sections 3 and 4. Summary will be made in section 5.

2. Numerical Model

A barotropic ocean with a constant depth is assumed (Fig. 2). We adopt a Cartesian coordinate system on a β plane with x-axis to east, y-axis to north. The vertically integrated vorticity equations under rigid lid approximation and hydrostatic balance by use of the ordinary notations are

$$\frac{\partial z}{\partial t} = -\frac{\partial uz}{\partial x} - \frac{\partial \upsilon z}{\partial y} - \beta \upsilon + A_h \nabla^2 z, \tag{2.1}$$

where volume transport function (ϕ) is related to u (v), the x-directed (the y-directed) component of velocity and the relative vorticity (z);

$$z = \frac{\partial \upsilon}{\partial t} - \frac{\partial u}{\partial y} = \frac{\partial}{\partial x}\left(\frac{1}{h}\frac{\partial \phi}{\partial x}\right) + \frac{\partial}{\partial y}\left(\frac{1}{h}\frac{\partial \phi}{\partial y}\right). \tag{2.2}$$

In order to see the dependence of the numerical solution on the model parameter, nondimensionalizing of Eq. (2.1) is carried out by $(x,y) = L(x^*, y^*)$, $t = (L/U)t^* = (1/\beta L)t^*$, where L is the representative width of the western boundary current and U is the representative velocity of the western boundary current. Then, (2.1) becomes (dropping primes)

$$\frac{\partial z}{\partial t} = -\mathrm{Ro}\left(\frac{\partial uz}{\partial x} + \frac{\partial \upsilon z}{\partial y}\right) - \upsilon + (1/\mathrm{Re})\nabla^2 z, \tag{2.3}$$

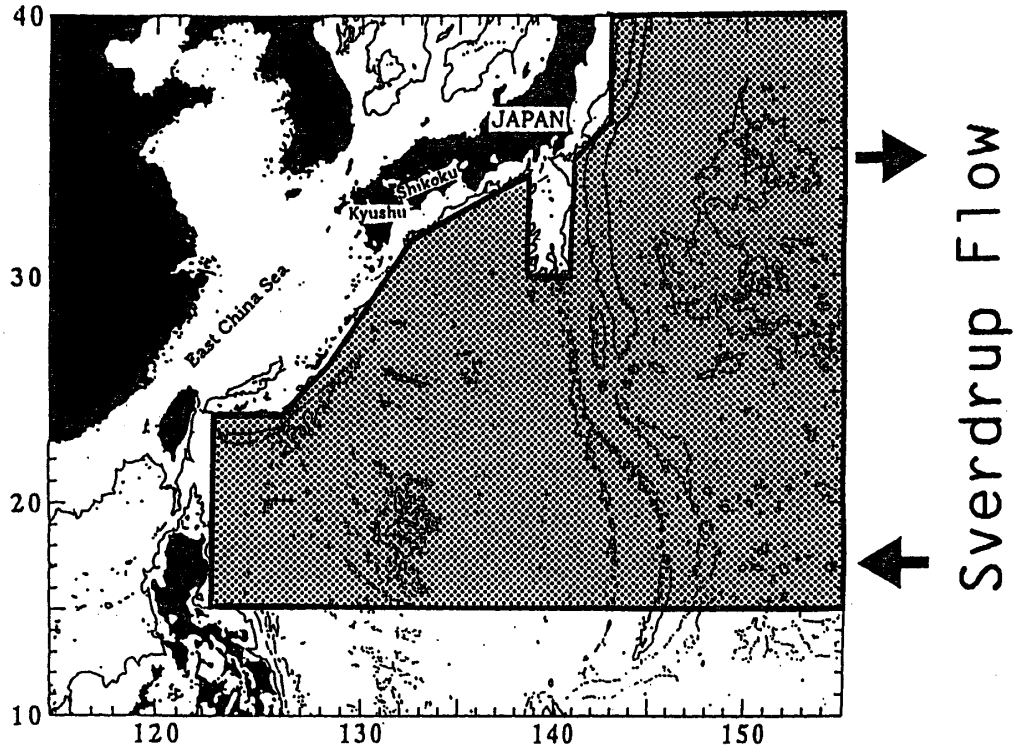

Fig. 2 Schematic view of the model ocean. In and outflow estimated as the Sverdrup transport is given at along 160° E.

where two nondimensional numbers are Reynolds number (Re=UL/Ah) and Rossby number (Ro=U/βL^2).

The system is driven by the observed in- and outflow estimated as the Sverdrup flow along 160° E by use of the wind stress over the period from 1961-1984 compiled by Kutsuwada and Teramoto[15]. Here, since the Ryukyu Current Extension is formed from winter to spring, the monthly mean Sverdrup transport in January and in April is given and dependence on the Rossby number is examined by changing the depths of the ocean such as 500m, 1000m, 2000m 4000m, 6000m and 8000m. On the other hand, dependence on the Reynolds Number is checked by two different coefficients of the horizontal eddy viscosity (Ah) with 5×10^6 cm^{2}sec^{-1} and 5×10^7 cm^{2}sec^{-1}. β, linear change rate of Coriolis Parameter, is assumed to be 2×10^{-13}cm^{-1}sec^{-1}.

In the present study, 24 cases of numerical models with different model character are examined. In the first step, monthly mean Sverdrup transport in winter (January) is given at the eastern boundary and six models with different depths are performed by use of two different coefficients of horizontal eddy viscosity (Table 1). These models with larger (smaller) eddy viscosity with the depth of 500m, 1000m, 2000m, 4000m, 6000m and 8000m are referred to as W05LE, W10LE, W20LE, W40LE, W60LE and W80LE (W05ME, W10ME, W20ME, W40ME, W60ME and W80ME), respectively (Table 1). In the second step, the monthly mean Sverdrup transport in Spring (April) is given and the similar 12 models with different depths and different coefficients of horizontal eddy viscosity are performed. They are referred to as S05LE and S05ME, in which S (spring) is used instead of W (winter) of the previous cases.

Ro and Re of each model is shown in Table 1, where U of 100 cmsec^{-1} and L of 200km of the Kuroshio

Table 1 Parameters of the numerical models

Run	In- and Outflow	Depth (m)	Ah in (2.1) ($\times 10^6$ cm^{2}sec^{-1})	Rossby No. ($U/\beta L^2$)	Reynolds No. (UL/Ah)
W05ME	Winter	500	50	2.50	80.0
W10ME	Winter	1000	50	1.25	40.0
W20ME	Winter	2000	50	0.63	20.0
W40ME	Winter	4000	50	0.31	10.0
W60ME	Winter	6000	50	0.21	6.7
W80ME	Winter	8000	50	0.16	5.0
W05LE	Winter	500	500	2.50	8.0
W10LE	Winter	1000	500	1.25	4.0
W20LE	Winter	2000	500	0.63	2.0
W40LE	Winter	4000	500	0.31	1.0
W60LE	Winter	6000	500	0.21	0.67
W80LE	Winter	8000	500	0.16	0.50
S05ME	Spring	500	50	1.75	56.0
S10ME	Spring	1000	50	0.88	28.0
S20ME	Spring	2000	50	0.44	14.0
S40ME	Spring	4000	50	0.21	7.0
S60ME	Spring	6000	50	0.15	4.7
S80ME	Spring	8000	50	0.11	3.5
S05LE	Spring	500	500	1.75	5.6
S10LE	Spring	1000	500	0.88	2.8
S20LE	Spring	2000	500	0.44	1.4
S40LE	Spring	4000	500	0.21	0.7
S60LE	Spring	6000	500	0.15	0.47
S80LE	Spring	8000	500	0.11	0.35

south of Japan are assumed for the case with a depth of 1000m and driven by winter in- and outflow (W10ME and W10LE). U of the cases driven by spring in- and outflow is 70% of that of those driven by winter in- and outflow, which is based on the fact that the Sverdrup in- and outflow of winter cases is 58.0 Sv (1 Sv$=10^{12}$cm^{3}sec^{-1}) and that of spring cases is 41. 1 Sv.

Viscous boundary conditions is imposed on the northwestern boundary, while a slip boundary condition is imposed on the other boundaries. In the numerical calculation, we adopt a rectangular grid with horizontal spacing of 24.80 km in west-east direction and 27.75 km in south-north direction. The numerical schemes of the basic equations are the same as in Sekine[16]. The initial condition of the volume transport function is given as

$$\begin{cases} \phi = \phi_0 \sin((\pi/2L)(x-x_0)) & \text{in the eastern side of } 145^\circ \text{ E,} \\ \text{and } \phi = 0 & \text{in the western side of } 145^\circ \text{ E,} \end{cases}$$

where ϕ_0 is the Sverdrup volume transport along 160° E estimated from 120° W, L and x_0 are the zonal distance between 145° E and 160° E and the x coordinate of 145° E, respectively.

3. Results with the winter Sverdrup In- and outflow

Result of W40LE is shown in Fig. 3. A stationary state is achieved by 30 days and a flow pattern is essentially similar to Munk solution modified by the topographic effect of the Izu Ridge. A wide and weak zonal flow is formed in the Shikoku Basin, which corresponds to the Ryukyu Current Extension. Hereafter, this flow pattern in the Shikoku Basin is referred to as the Munk Pattern.

As the similar time change is carried out in all the case with larger eddy viscosity, only their stationary state is shown in Fig. 4. Similar flow pattern to W40LE is seen in W20LE (Fig. 4c), W60LE (Fig. 4e) and W80LE (Fig. 4f). A larger volume transport of the subtropical circulation is formed in W05LE (Fig. 4a) and W10LE (Fig. 4b) and the maximum volume transport region is shifted northward.

The time change in the volume transport function of W05ME is shown in Fig. 5. A large subtropical circulation with the large volume transport is formed and the strong eastward current is generated in the northern region of the subtropical circulation. A strong eastward flow with the northward intensification is seen in the Shikoku Basin and the Ryukyu Current Extension is not formed, while the ordinary Kuroshio path along the Japanese Coast is enhanced in this case. This flow pattern in the Shikoku Basin is referred to as the Super Nonlinear Pattern.

In comparison with W05ME, the amplification of the current meander is more significant in W10ME (Fig 6), while the volume transport of the subtropical circulation is weakened. Namely, the volume transport of the subtropical circulation of W05ME exceeds 100 Sv (Fig. 5), but the subtropical circulation of W10ME is divided into two or three eddies. The wavelength of the stationary Rossby wave $2\pi (U/\beta)^{1/2}$ of the meander east of Japan of W10ME is shorter than that of W05ME and a closed anticyclonic eddy is formed in the Shikoku Basin. It is thus suggested that as for the W05ME (Fig. 5) half of the the wavelength of the meander is longer than the zonal scale of the Shikoku Basin, however that of W10ME is almost equal to the zonal scale of the Shikoku Basin and the stable anticyclonic eddy with large volume transport is formed in the Shikoku Basin. The current pattern with a prominent anticyclonic eddy formed in W10ME is hereafter referred to as Nonlinear Pattern.

In W20ME (Fig. 7), the amplitude and the volume transport of the anticyclonic eddies accompanied by the large meander east of Japan are decreased. Although the anticyclonic eddy does not completely occupies all the area of the Shikoku Basin, the Nonlinear Pattern seems to be formed in this case. Decrease in the amplitude and volume transport is much enhanced in W40ME (Fig. 8). In the Shikoku Basin, mean flow of W40ME separates from the coast east of Shikoku and a prominent eastward flow corresponding the Ryukyu Current Extension is formed. The flow pattern of the W40ME in the Shikoku Basin is similar to Moore solution[17] shown from the weak nonlinear analytical theory of the western boundary current. This flow pattern in the Shikoku Basin is referred to as the Moore Pattern.

As almost similar patterns to W40ME is obtained in W60ME and W80ME, their stational state is shown in Fig. 9ef, together with those of all the models with the small eddy viscosity driven by winter Sverdrup

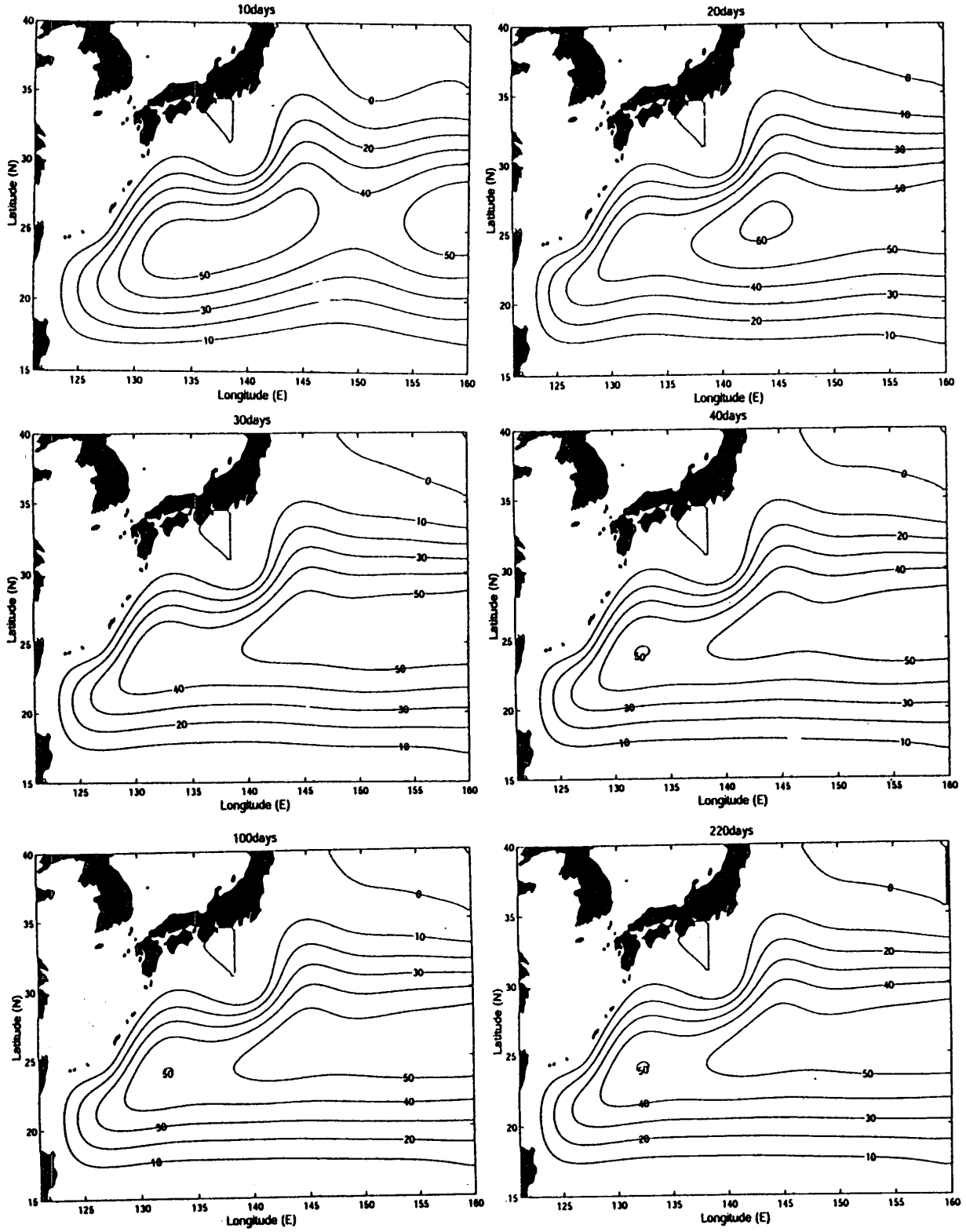

Fig. 3 Results of the numerical model of W40LE shown by isopleth of the volume transport function. The contour interval of the volume transport function is 10 Sv. The integrated time period is shown at the top of each panel.

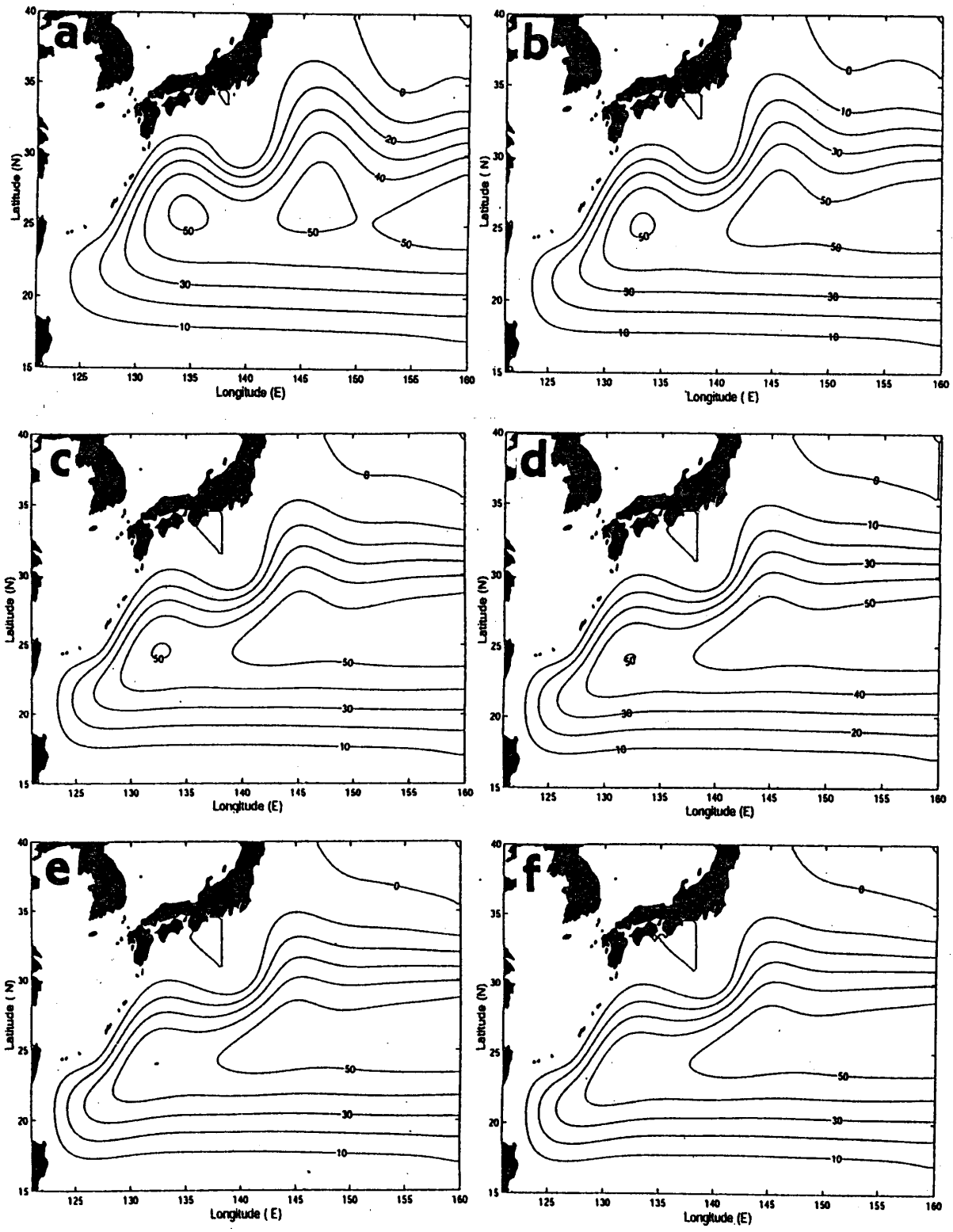

Fig. 4 Results of the numerical models with the large eddy viscosity driven by winter Sverdrup in- and outflow. (a) W05LE, (b) W10LE, (c) W20LE, (d) W40LE, (e) W60LE and (f) W80LE. Descrption of each model is the same as in Fig. 3.

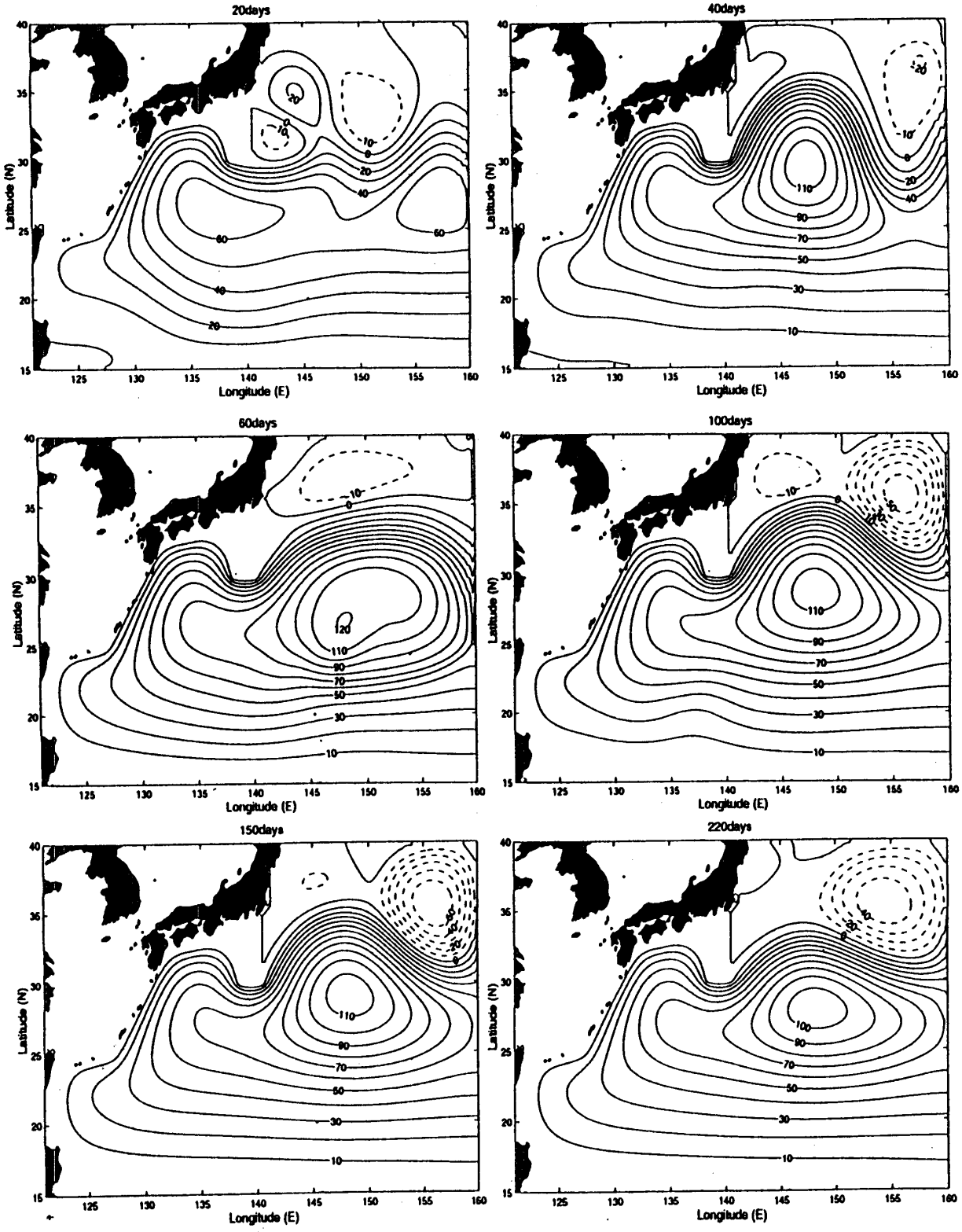

Fig. 5 As in Fig. 3, but for the case of W05ME. Regions with negative volume trasnport fuction are shown by broken lines.

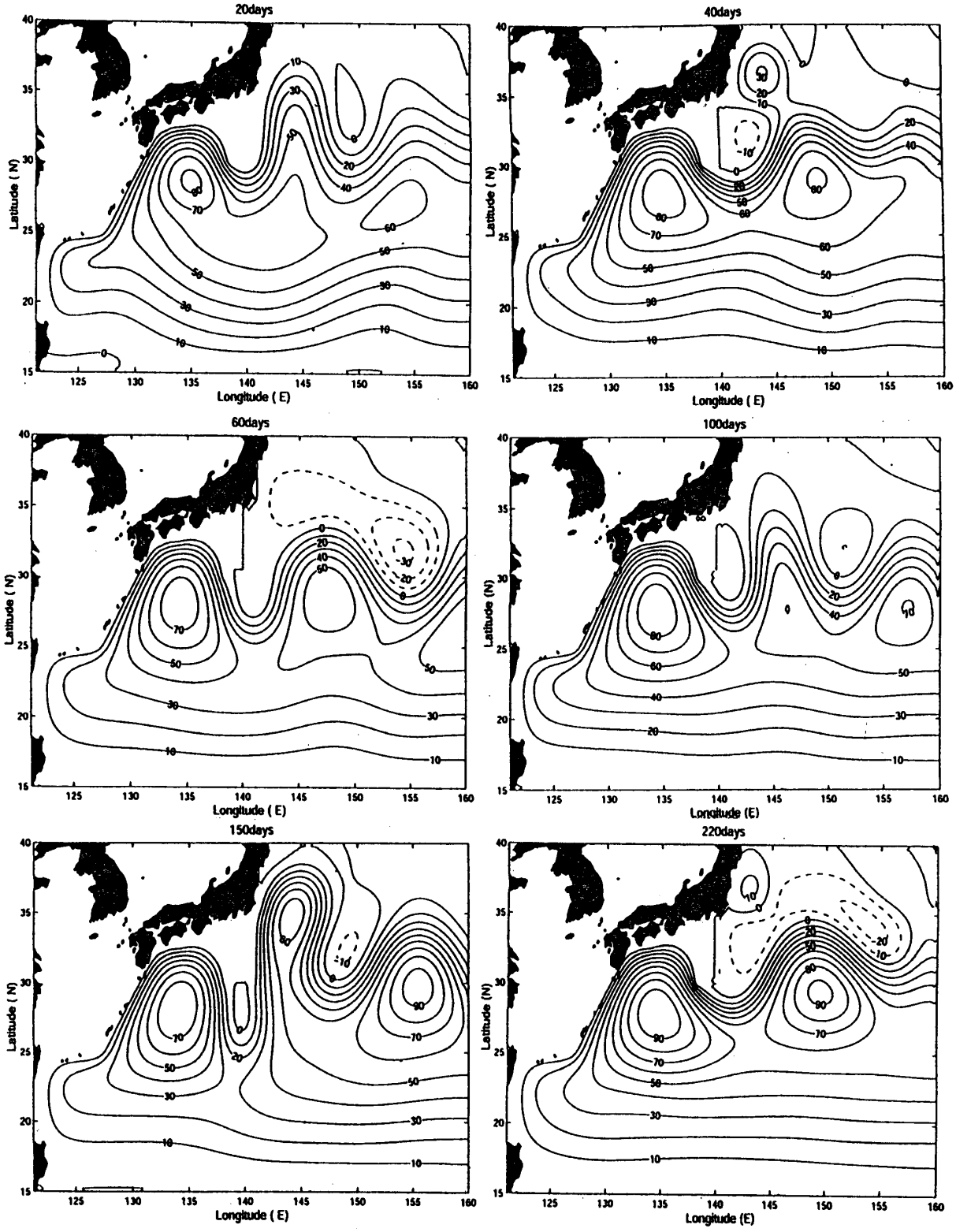

Fig. 6 As in Fig. 5, but for the case of W10ME.

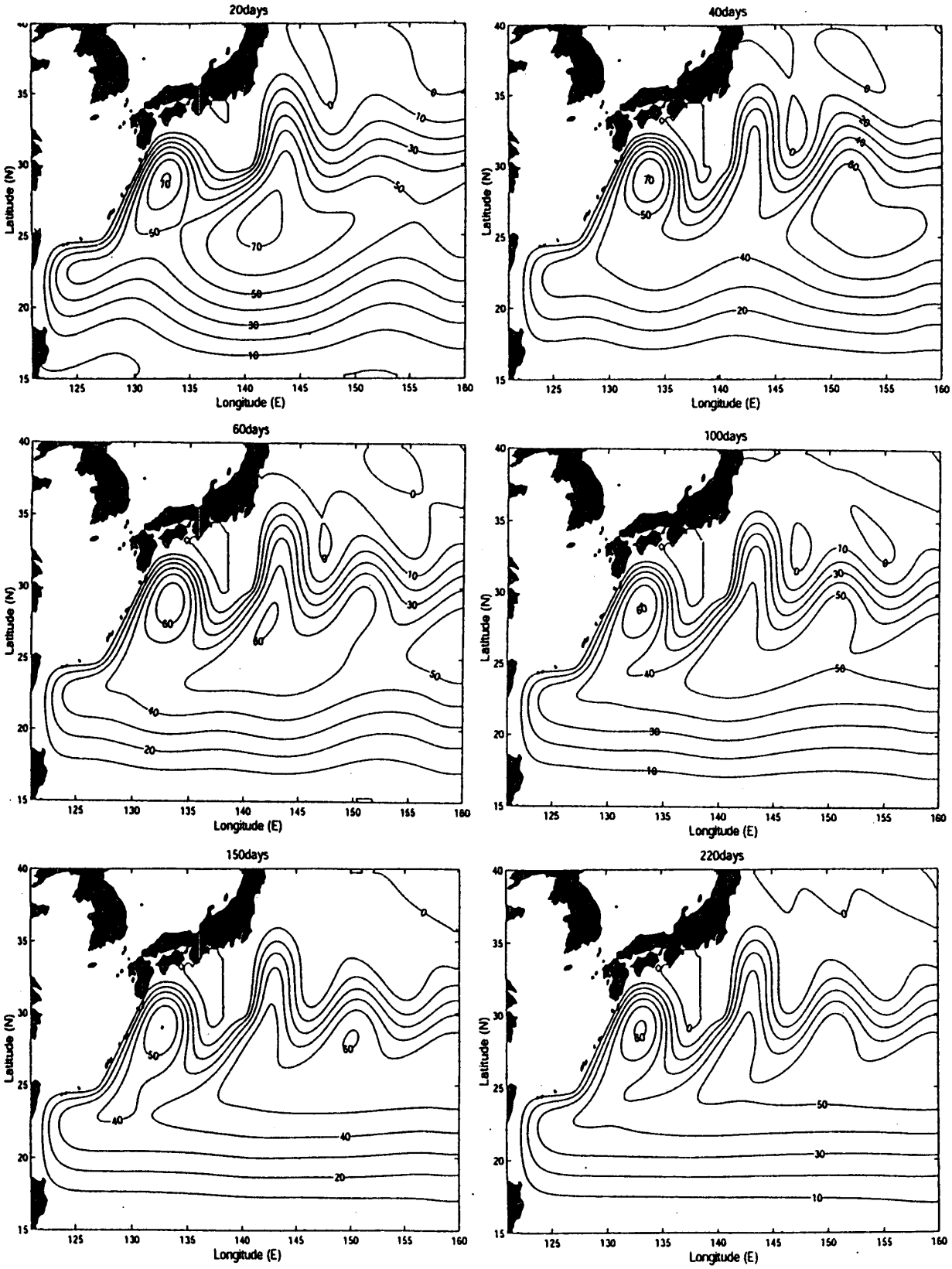

Fig. 7 As in Fig. 5, but for the case of W20ME.

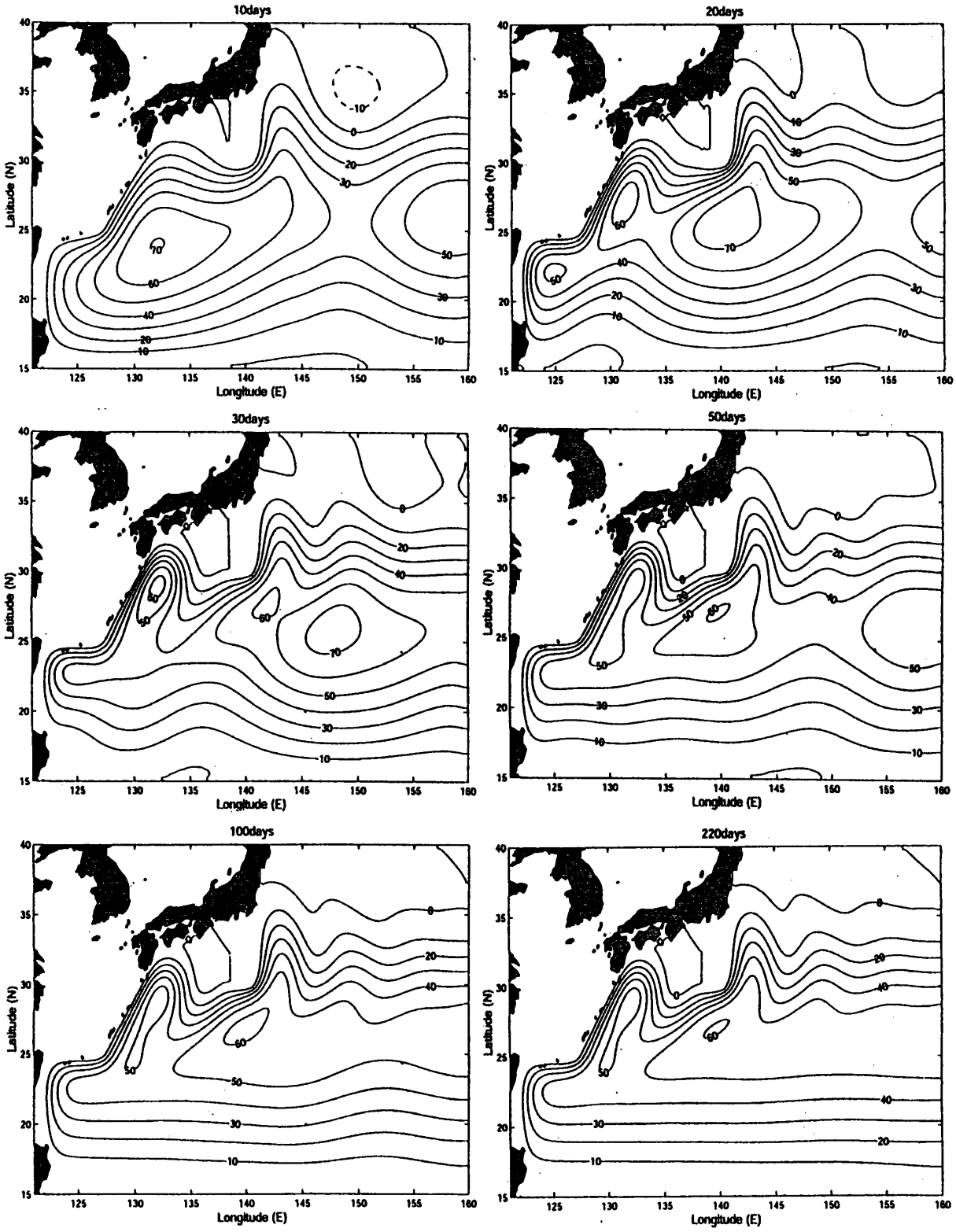

Fig. 8 As in Fig. 5, but for the case of W40ME.

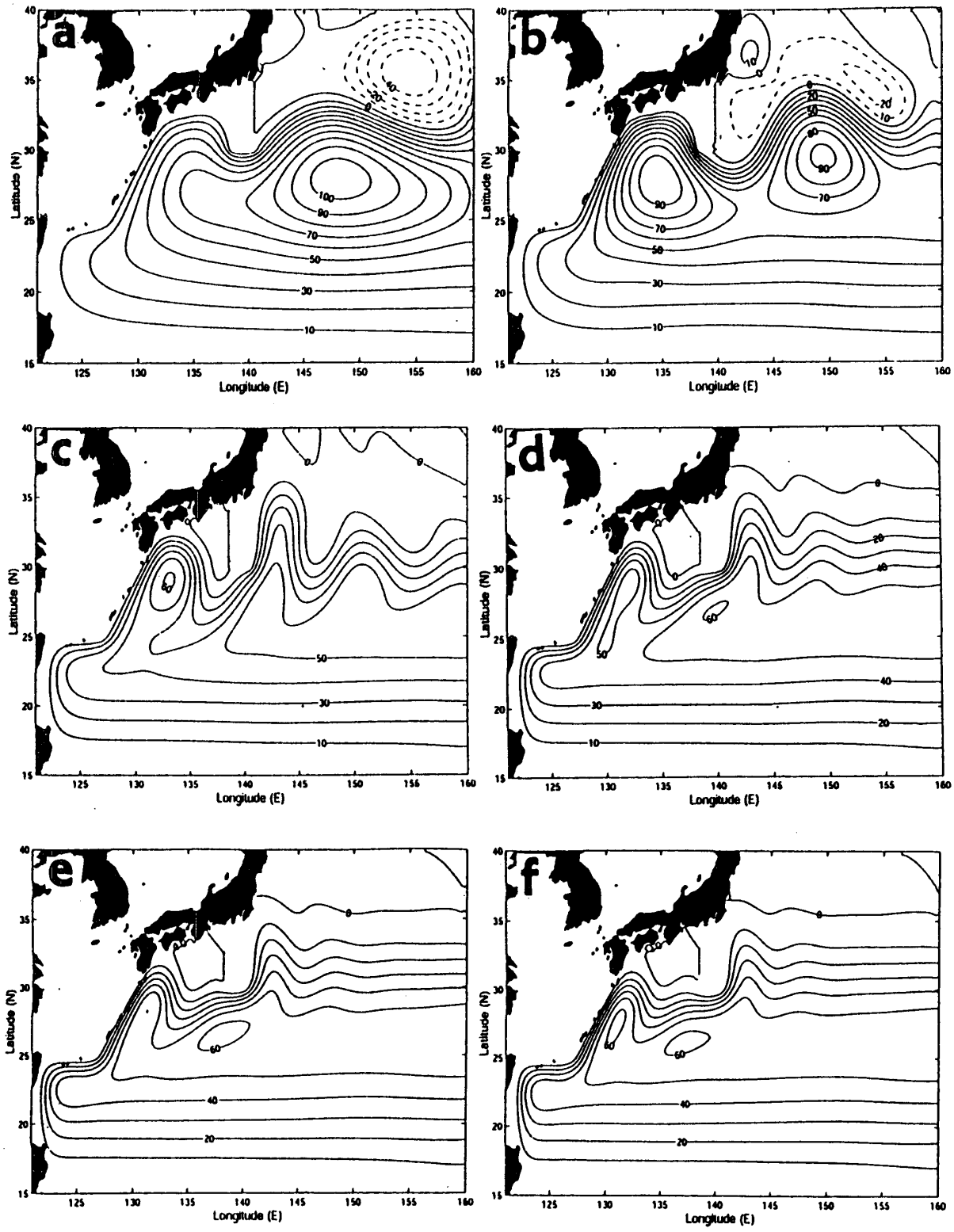

Fig. 9 As in Fig. 4, but for the numerical models with the small eddy viscosity driven by winter Sverdrup in- and outflow. (a) W05ME, (b) W10ME, (c) W20ME, (d) W40ME, (e) W60ME and (f) W80ME.

in- and outflow. It is seen from Fig. 9def that the separation of the current path occurs east of Kyushu in W40ME (Fig. 9d), the separation point shifts weakly southward in W80ME, which implies that the northward shift of the anticyclonic eddy is weakened as the in- and outflow Sverdrup flow is decreased. In comparison with W40ME, W60ME and W80ME, the separation of the current path does not occur in W05ME (Fig. 9a) by the wide strong eastward flow and in W10ME (Fig. 9b) by the large anticyclonic eddy in the Shikoku Basin. Intermediate flow pattern between W10ME and W40ME is seen in W20ME (Fig. 9c), the formation of the completely isolated anticyclonic in the Shikoku Basin implies that the Nonlinear Pattern is suitable for this case.

4. Results with the spring Sverdrup in- and outflow

Munk Pattern is obtained in all the models with the large eddy viscosity (Fig. 10). Although the maximum transport is found in a southern latitude to the Izu Ridge in the models driven by winter Sverdrup in- and outflow (Fig. 4), the maximum volume transport function is in the eastern side of the Izu Ridge in this case. This is due to the northward shift of the spring Sverdrup in- and outflow.

Although the northward shift of the subtropical circulation is clear between W05LE (Fig. 4a) and W80LE (Fig. 4f), the northward shift is unclear between S05LE (Fig. 10a) and S80LE (Fig. 10e). The difference is caused by the weak spring Sverdrup in- and outflow compared with the winter in- and outflow. Namely, the total volume transport of the winter in- and outflow is 55 Sv, while the spring in- and outflow is 40 Sv. Furthermore, the eastward volume transport in the southern latitude to the Izu Ridge is 55 Sv for the winter case, but that of the spring case is 34 Sv. It is thus suggested that the larger northward shift of the subtrpical circulation in winter is due to the large Sverdrup in- and outflow in winter.

The volume transport of the subtropical circulation of S05ME (Fig. 11) is weak in comparison with that of W05ME (Fig. 5). On the other hand, the large amplitude meander is formed in the eastern area of Japan. Because a clear anticyclonic eddy is not formed in the Shikoku Basin, the Super Nonlinear Pattern is essentially generated in this case. In contrast to this, the anticyclonic eddy is gradually enhanced in S10ME (Fig. 12) and a typical Nonlinear Pattern is formed in this case. The difference between S05ME and S10ME is common to that between W05ME (Fig. 5) and W10ME (Fig. 6); $2\pi(U/\beta)^{1/2}$ of W05ME and S05ME is larger than the zonal length of the Shikoku Basin (L), however, that of W10ME and S10ME is almost equal to L and the anticyclonic eddy can develop gradually.

Moore Pattern is formed in S20ME (Fig. 13). A critical point between the Nonlinear Pattern and the Moore Pattern exists between S10ME and S20ME, which is different from the winter case (between W20SE and W40SE). It is also seen from Fig. 13 that the only an anticyclonic eddy is formed east of Japan and the westward intensification is more enhanced in comparison with S10ME (Fig. 12).

The westward intensification is furthermore clear in S40ME (Fig. 14). A weak northward shift of the anticyclonic eddy is found in the Shikoku Basin and the total flow pattern of S40ME shows a gradual approach from Moore Pattern to Munk Pattern. The flow pattern in the Shikoku Basin is essentially similar to W60ME (Fig. 8) and W80ME (Fig. 9) and the Ryukyu Current Extension appears clearly in these cases.

As the similar numerical solution to S40ME is obtained in S60ME and S80ME, their stationary state is shown in 5ef. The decreasing rate of the Munk layer thickness $(Ah/\beta)^{1/3}$ from the large eddy viscosity to

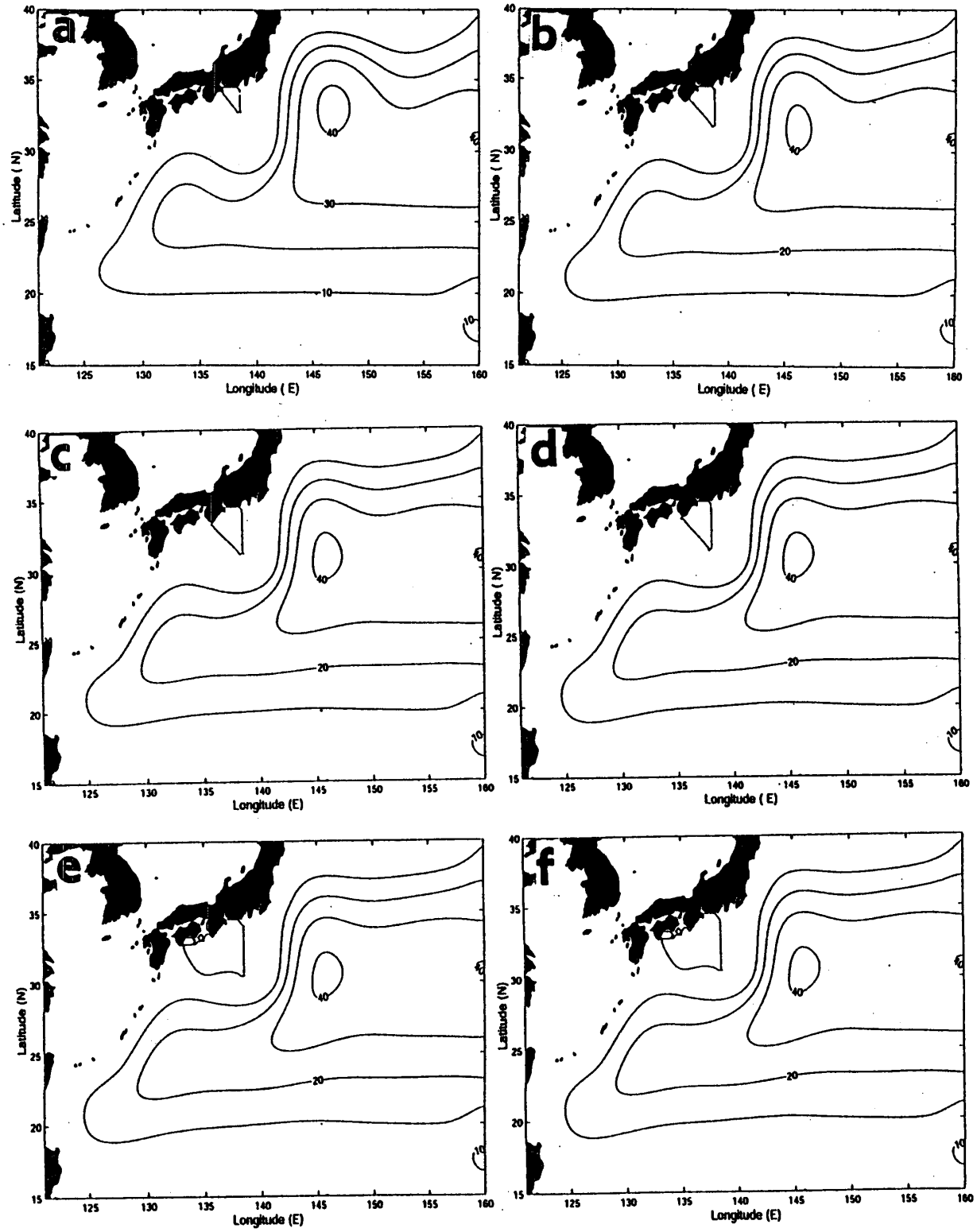

Fig. 10 As in Fig. 4, but for the numerical models with large eddy viscosity driven by spring Sverdrup transport. (a) S05LE, (b)S10LE, (c) S20LE, (d) S40LE, (e) S60LE and (f) S80LE.

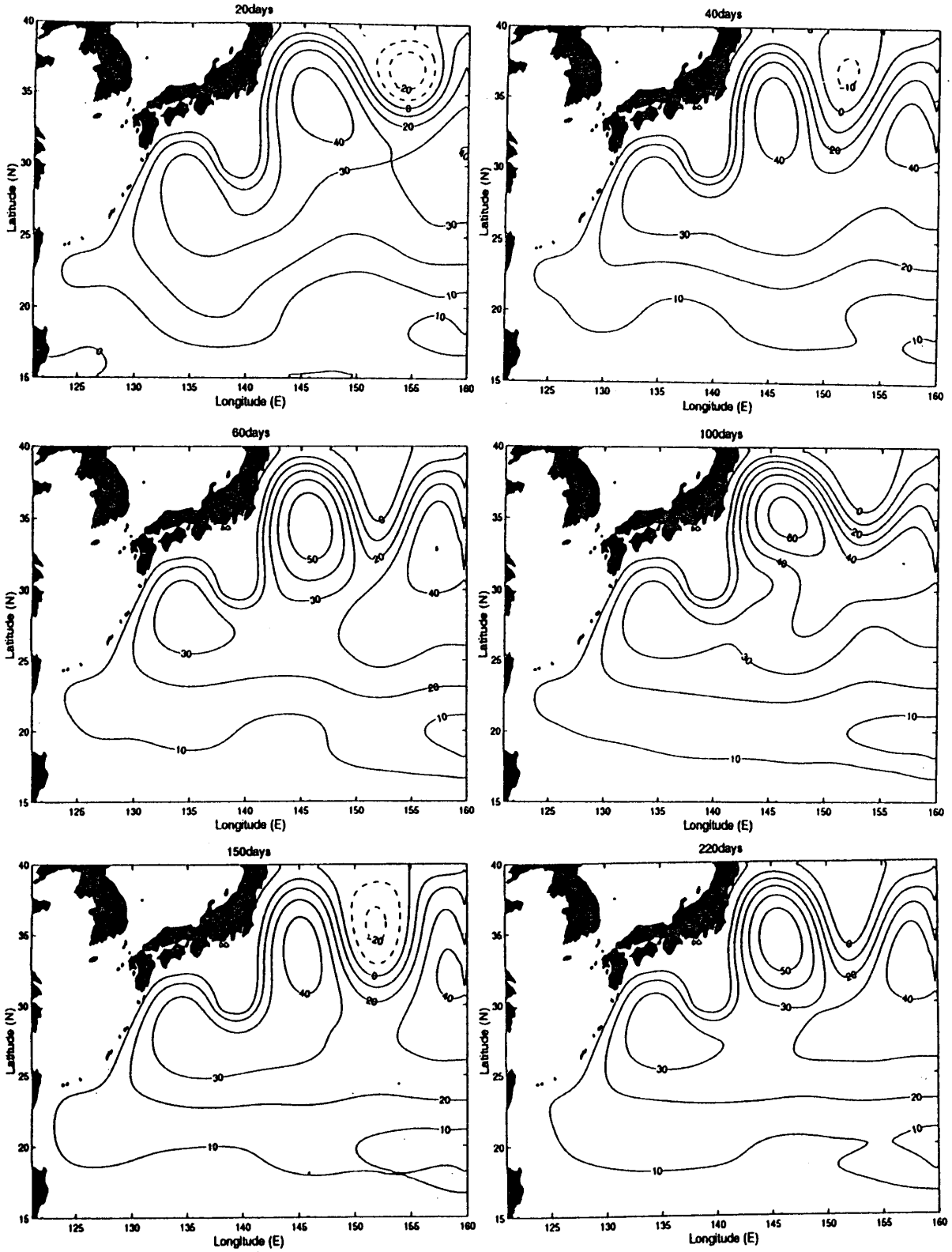

Fig. 11 As in Fig. 5, but for the case of S05ME.

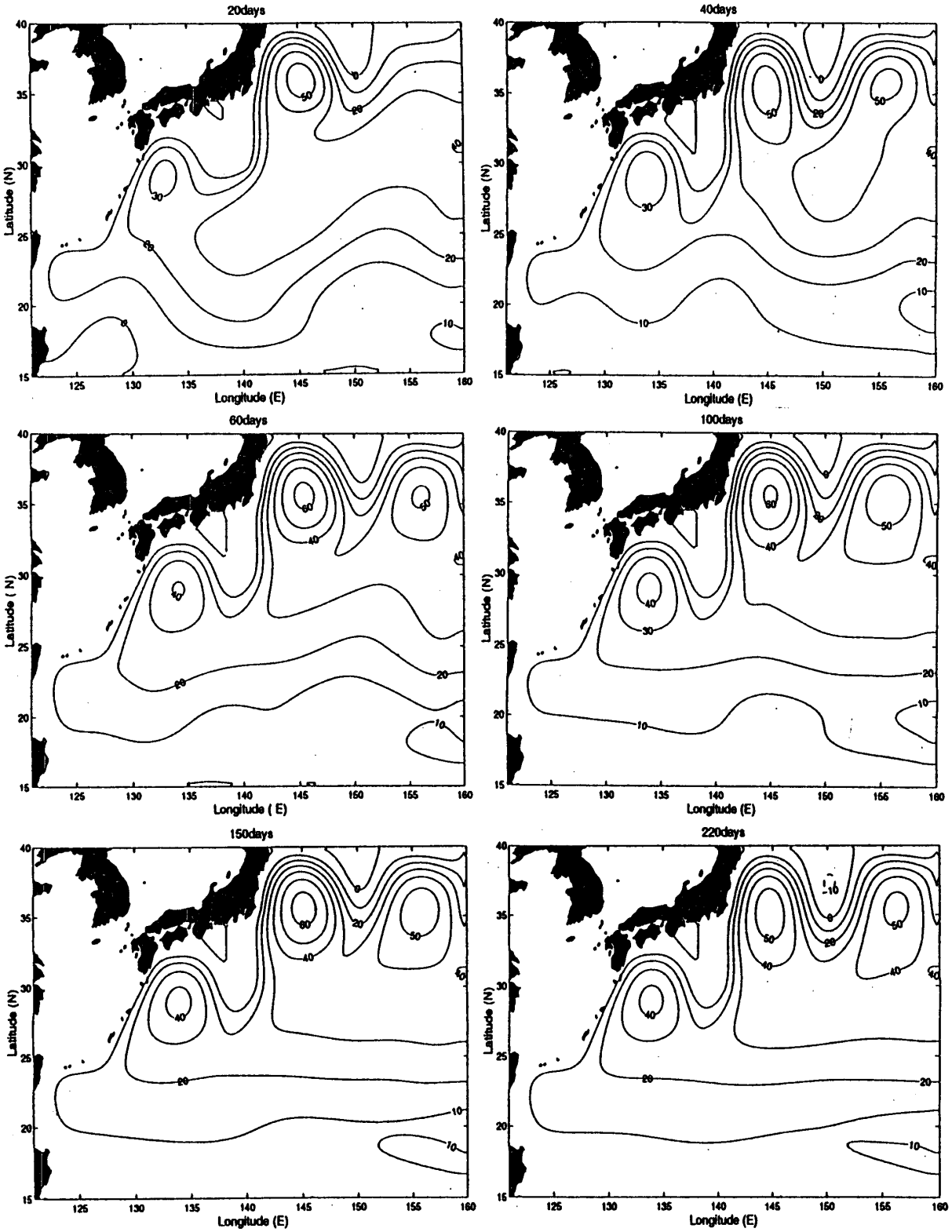

Fig. 12 As in Fig. 5, but for the case of S10ME.

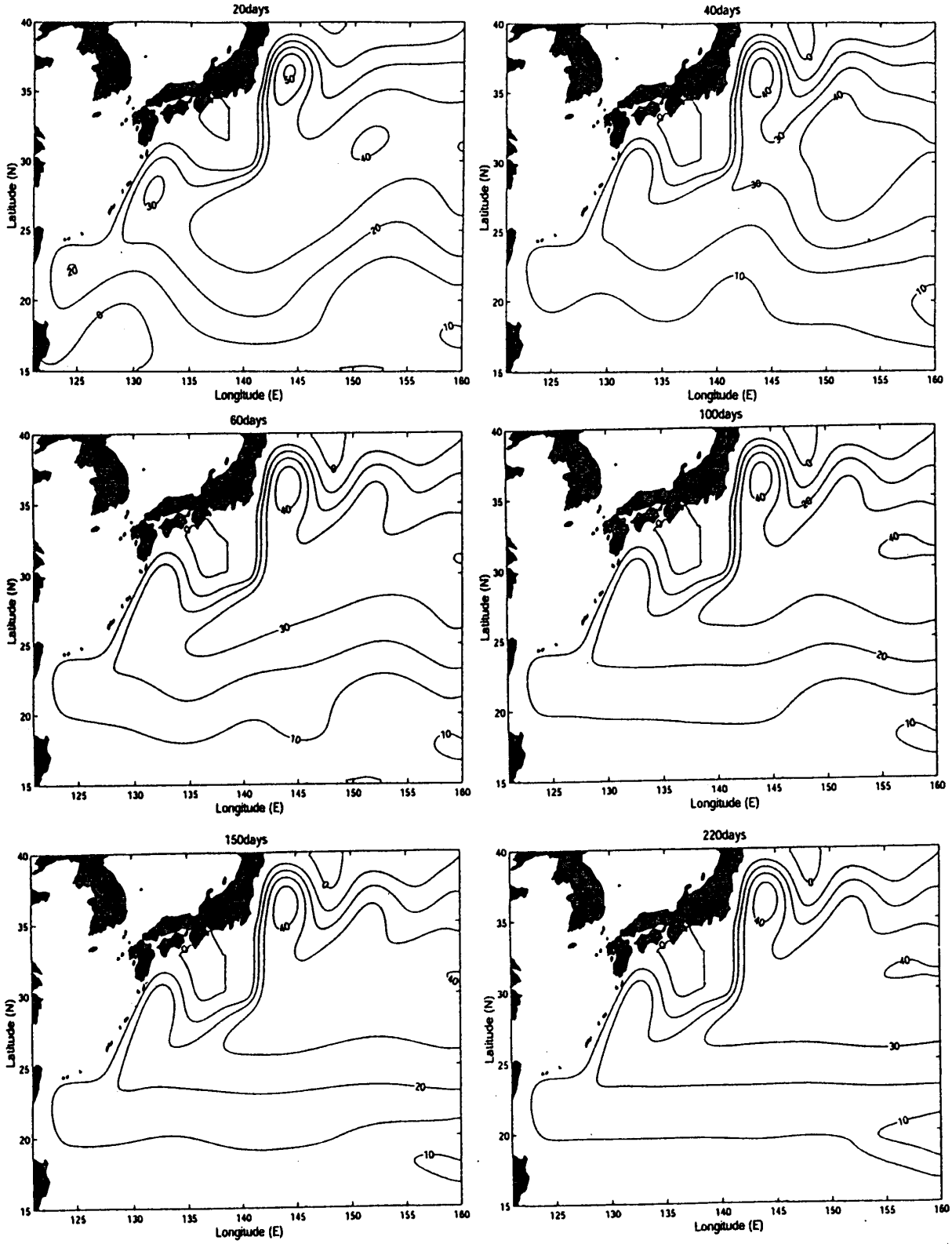

Fig. 13 As in Fig. 5, but for the case of S20ME.

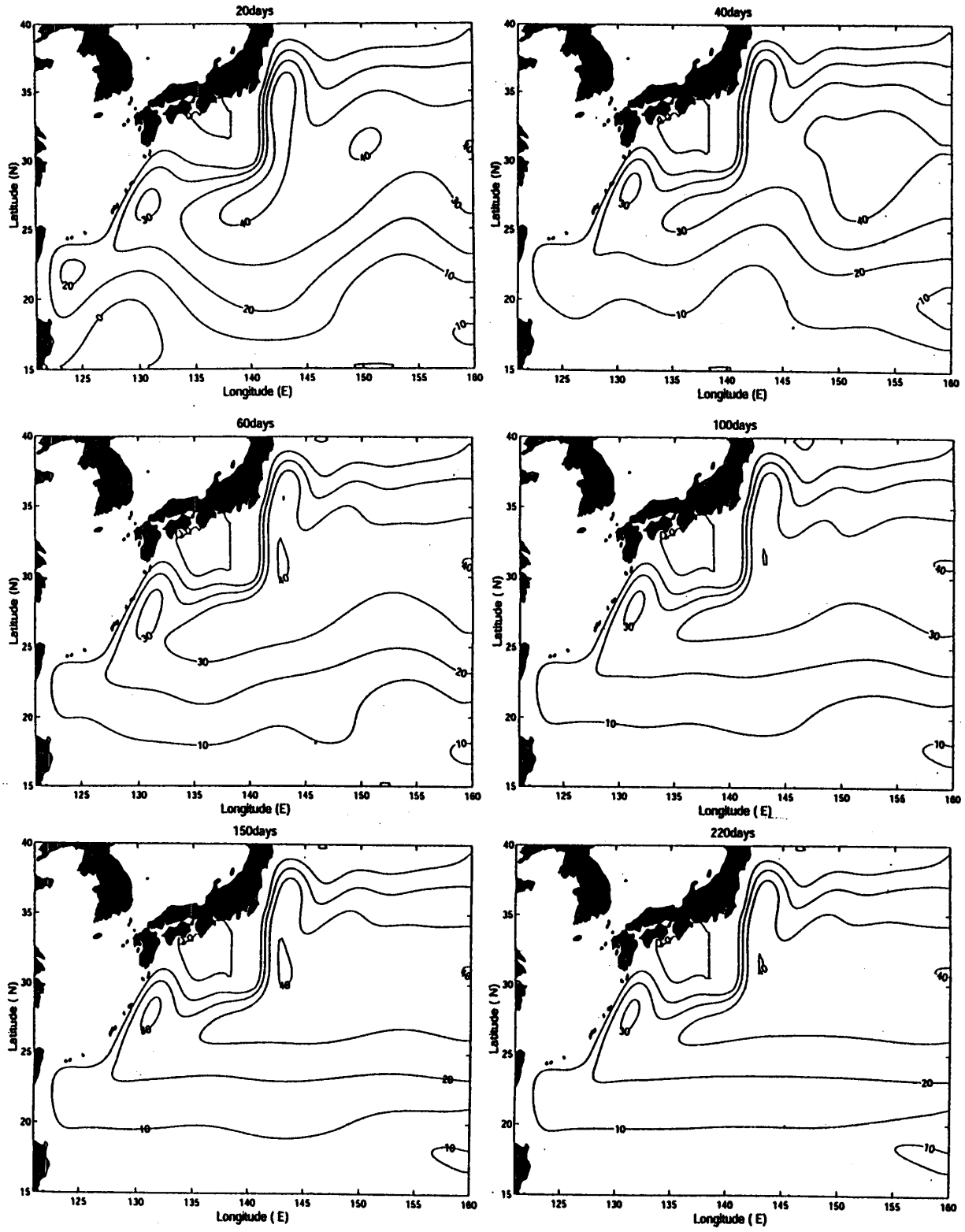

Fig. 14 As in Fig. 5, but for the case of S40ME.

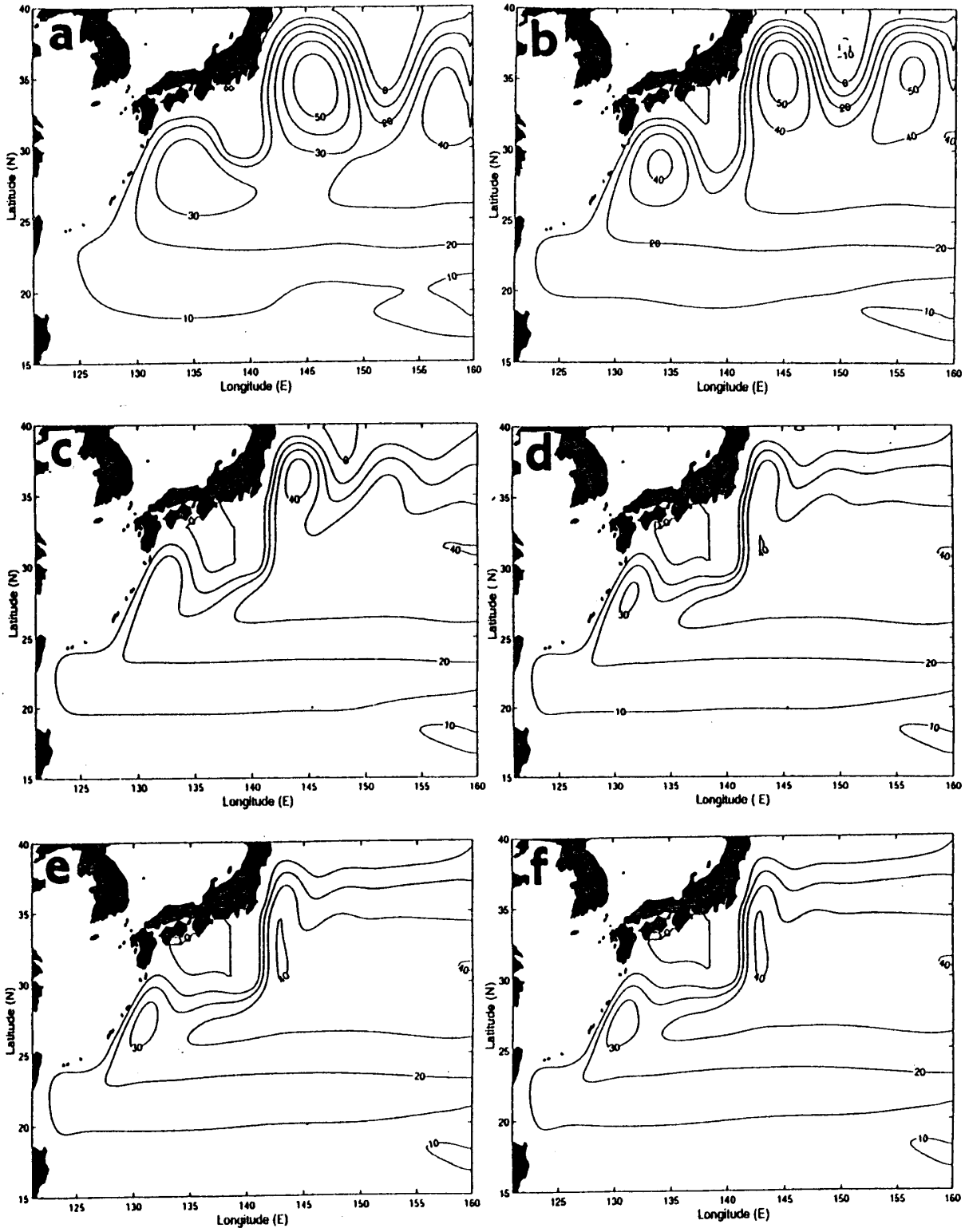

Fig. 15 As in Fig. 4, but for the numerical models with the small eddy viscosity driven by spring Sverdrup transport. (a) S05ME, (b)S10ME, (c) S20ME, (d) S40ME, (e) S60ME and (f) S80ME.

the small eddy viscosity is 2. 15. The flow pattern of S60ME and S80ME is essentially considered as the Munk Pattern, if we consider the decreasing rate of the Munk Layer. On the whole, it is resulted from Fig. 15 that the Super Nonlinear Pattern is obtained in S05SE, the Nonlinear Pattern in S10ME, the Moore Pattern in S20ME and the Munk Pattern in S40ME, S60ME and S80ME. The Ryukyu Current Extension is clear in the Moore and Munk Patterns, but it is not formed in the Super Nonlinear and Nonlinear Patterns.

5. Summary

Because the barotropic oceanic response is dominant for the seasonal change in wind stress, there exist two western boundary currents along the eastern continental slope off the Nansei Islands (Ryukyu Current)[1)-2)] and along the eastern side of the Izu Ridge[6)] from late winter to spring. Therefore, an connecting current from the Ryukyu Current to the western boundary current along eastern side of the Izu Ridge, referred to as the Ryukyu Current Extension, is predicted. Flow characteristics of the Ryukyu Current Extension is examined by use of the numerical models with linear and weak nonlinear parameters, as a Part I of this study. Main results of the numerical experiment is as follows:

(1) There exist four type of the current patterns in the Shikoku Basin, which are referred to as the Munk Pattern, Moore Pattern, Nonlinear Pattern and Super Nonlinear Pattern. The Ryukyu Current Extension is clearly formed in the Munk Pattern and the Moore Patterns, but it is unclear in the Super Nonlinear Pattern and Nonlinear Pattern.

(2) If the coefficient of the horizontal eddy viscosity is large, only Munk Pattern is formed. If the eddy viscosity is decreased, the Munk and Moore Patterns are formed in the small in- and outflow models (deep models), while the Nonlinear Pattern and the Super Nonlinear Pattern appear in the models driven by the large in- and outflow (shallow models) and in that driven by the largest in- and outflow (shallowest model), respectively.

(3) The critical point between the Nonlinear Pattern and Moore Pattern is between W20SE and W40SE in the models driven by the winter in- and outflow, but that is between S10SE and S20SE in the models driven by the spring in- and outflow. The difference is due to the larger (smaller) in- and outflow velocity in winter (spring). The northward shift of the Sverdrup flow in spring in- and outflow yields a northward development of the subtropical circulation south of Japan, which has a much influence on the flow pattern of the subtropical circulation in spring.

It is thus demonstrated that the appearance of the Ryukyu Current Extension depends on the model parameterization such as the Reynolds number (eddy viscosity) and the Rossby number (representative velocity of the western boundary current controlled by the depth of the ocean in the barotropic model). To draw firm conclusion, some general nonlinear cases should be furthermore examined and the results of such an numerical experiment will be presented in the Part II of this work.

Acknowledgment

I would like to thank Mr.Jun Furui the Faculty of Bioresources, Mie University for his help in numerical calculation and drawing some figures.

References

1) SEKINE, Y. and K. KUTSUWADA. (1994) Seasonal variation in volumetransport of the Kuroshio south of Japan. J. Phys. Oceanogr., **24**, 261−272.
2) KAGIMOTO, T. and T. YAMAGATA. (1997) Seasonal transport variation of the Kuroshio: An OGCM simulation. J. Phys. Oceanogr., **27**, 403−418.
3) PEDOLOSKY, J. (1979) "Geophysical fluid dynamics". Springer Verlag, New York, 624pp.
4) GILL, A. E. (1982) "Atmosphere-ocean dynamics", Academic press, New York, London, 662pp.
5) IMAWAKI, S., H. UCHIDA, H. ICHIKAWA, M. FUKASAWA, S. UMATANI and ASUKA Group. (2002) Satellite altimeter monitoring the Kuroshio transport south of Japan. Geophys. Res. Lett., **28**, 17−20.
6) ISOBE, A. and S. IMAWAKI. (2002) Annual variation of the Kuroshio transport in a two-layer numerical model with a ridge. J. Phys. Oceanogr., **32**, 994−1009.
7) KAWABE, M. (2001) Interannual variations of sea level at the Nansei Islands and volume transport of the Kuroshio due to wind changes. J. Oceanogr., **57**, 189−205.
8) HASUNUMA, K. and K. YOSHIDA. (1978) Splitting of the subtropical gyre inthe western North Pacific. J. Oceanogr. Soc. Japan, **34**, 160−172.
9) EBUCHI, N. and K. HANAWA (2000): Mesoscale eddies observed by TOLEX-ADCP and TOPEX/POSEIDON altimeter in the Kuroshio recirculation region south of Japan. J. Oceanogr., **56**, 43−57.
10) EBUCHI, N. and K. HANAWA (2003) Influence of mesoscale eddies on variation of the Kuroshio path south of Japan. J. Oceanogr., **59**, 25−36.
11) SEKINE, Y., S. WATANABE and F. YAMADA (2000) Topographic effect of the Izu Ridge on the horizontal distribution of the North Pacific Intermediate Water. J. Oceanogr., **56**, 429−438.
12) SEKINE, Y. and S. MIYAMOTO (2002): Influence of the Kuroshio flow on the horizontal distribution of the North Pacific Intermediate Water in the Shikoku Basin. J. Oceanogr., **58**, 611−616.
13) DERUIJTER, W. P. (1982) Asymptotic analysis of the Agulhas and Brazil Current system. J. Phys. Oceanogr., **12**, 361−373.
14) DERUIJTER, W. P. and D. B. BOUDRA. (1985) The wind-driven circulation inthe south Atlantic-Indian Ocean. I. Numerical model. Deep-Sea Res., **32**, 557−574.
15) KUTSUWADA, K. and T. TERAMOTO (1987) Monthly maps of the surface wind stress fields over the North Pacific during 1961−1984. Bull. Ocean Res. Inst. Univ. Tokyo, **24**, 1−100.
16) SEKINE, Y. (1988) Coastal and bottom topographic effect on the path dynamics of the western boundary current with special reference to the Kuroshio south of Japan. La mer, **26**, 99−114.
17) MOORE, D. W. (1963) Rossby waves in ocean circulation. Deep-Sea Res., **10**, 735−747.

新しい海流である琉球海流続流に関する数値モデル実験 第1部 線形および弱非線形モデル

関 根 義 彦

三重大学生物資源学部

風の海面応力の季節変動については海洋の順圧応答が卓越し，北太平洋の亜熱帯循環では南西諸島の東にある大陸棚斜面に沿う琉球海流といわれる西岸境界流と伊豆海嶺の東にある西岸境界流の存在が晩冬から春にかけて指摘されていた。したがってこの二つの西岸境界流を接続する海流の存在が予知され，ここでは琉球海流続流と呼ぶ。この琉球海流続流の流れの特性を見るため，順圧モデルを仮定して冬と春のスヴェルドラップバランスした流れで駆動する幾つかの数値モデル実験を行った。本論では線形および弱非線形のモデルパラメータを与えた数値モデルの結果をまとめた。その結果，四国海盆ではムンク型，ムーア型，非線形型，超非線形型の 4 つの流れのパターンが存在することが示された。大きい渦粘性係数の場合にはムンク型のみが生じること，小さい渦粘性係数の場合には深さで制御される流入出速度が小さい場合にはムーア型が生じ，流入出速度が大きい場合には非線形型，流入出速度が最大の場合には超非線形型が生じることが示された。さらに，琉球海流続流はムンク型とムーア型の場合に明瞭に出現するが，非線形型と超非線形型の場合には不明確となることが示された。